Minimal Molecular Building Blocks for Screening in Quasi-Two-Dimensional Organic–Inorganic Lead-Halide Perovskites

Jack McArthur[1,2], Marina R. Filip[3], Diana Y. Qiu[1,4]*

1. Department of Physics, Yale University, New Haven, Connecticut 06520, USA

2. Department of Physics, University of California at Berkeley, California 94720, USA

3. Department of Physics, University of Oxford, Clarendon Laboratory, Oxford OX1 3PU, United Kingdom

4. Department of Mechanical Engineering and Materials Science, Yale University, New Haven, Connecticut 06520, USA

TOC Graphic

PbBr$_4^{2-}$ NMA$^+$ (NMA)$_2$PbBr$_4$

e$^-$
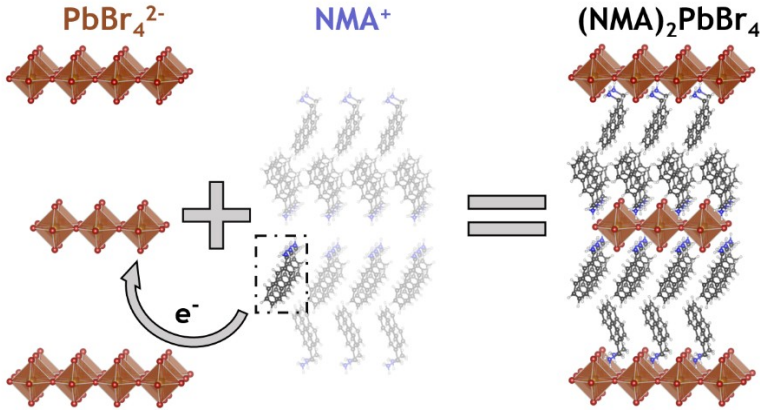
ABSTRACT *Layered hybrid organic-inorganic lead halide perovskites have intriguing optoelectronic properties*, *but some of the most interesting perovskite systems, such as defective, disordered, or mixed perovskites, require multiple unit cells to describe and are not accessible within state-of-the-art ab initio theoretical approaches for computing excited states. The principal bottleneck is the calculation of the dielectric matrix, which scales formally as $O(N^4)$. We develop here a fully ab initio approximation for the dielectric matrix, known as IPSA-2C, in which we separate the polarizability of the organic/inorganic layers into minimal building blocks, thus circumventing the undesirable power-law scaling. The IPSA-2C method reproduces the quasiparticle band structures and absorption spectra for a series of Ruddlesden-Popper perovskites to high accuracy, by including critical non-local effects neglected in simpler models, and sheds light on the complicated interplay of screening between the organic and inorganic sublattices.*

Layered hybrid organic-inorganic perovskites are an emerging class of quasi-low dimensional optoelectronic materials that have attracted widespread interest due to their highly tunable structures, relative stability, and facile synthesis in bulk, monolayer, and heterostructure forms.[1-

[3] A prototypical class of these perovskites is the Ruddlesden-Popper (RP) phase, with the generic formula $A'_{n-1}A_2B_nX_{3n+1}$, (A and A' = monovalent cations, B = divalent metal cation, and X = halogen or oxygen ion) that alternates n layers of BX_6 octahedra with a layer of organic cations $A = RNH_3$.[4, 5]

The interest in RP perovskites has generated a comprehensive body of work on their electronic and optical properties.[6, 7] Excitons localized within the inorganic metal-halide layers experience strong dielectric and quantum confinement effects, giving rise to large exciton binding energies,[8-10] and the self-trapping of excitons on the soft inorganic lattice is a widely proposed mechanism for the highly Stokes-shifted luminescence observed in many RP perovskites.[11] The choice of organic species can also significantly affect the dielectric and optical properties of hybrid perovskites.[2, 12] For instance, some molecules with extended conjugated systems have singlet or triplet levels that excitons can decay to, opening new possible emission pathways.[13]

The excitonic properties of layered hybrid perovskites exhibit a complex dependence on dielectric screening, defects, lattice distortions, and coupling between organic and inorganic layers. Understanding these relationships requires a predictive, *ab initio* description of the excited-state properties that considers dynamic and local-field effects at a level beyond density functional theory (DFT). *Ab initio* many-body perturbation theory (MBPT) is a state-of-the-art approach for understanding excited-state properties, including single-quasiparticle (QP) excitations within the *GW* approximation[14, 15] and optical excitations within the *GW* plus Bethe-Salpeter Equation (*GW*-BSE) approach[16, 17]. However, there have only been a small number of

GW and *GW*-BSE calculations on layered perovskites,[4, 18, 19] largely due to the computational cost of such techniques and the relatively large unit cells of layered perovskites (often hundreds of atoms). Moreover, some of the most interesting perovskite systems, such as defective, disordered, or mixed perovskites, require multiple unit cells to describe and are not currently accessible within conventional *ab initio* MBPT approaches. To overcome this barrier, theoretical calculations frequently apply MBPT within simplified models. For instance, Ref. [20] makes use of a classical electrostatic model for the screening, and Ref. [19] treats a model lead-halide perovskite structure where the usual organic spacer molecules are replaced by Cs atoms.[21, 22] These approaches provide qualitative understanding of certain perovskite optical properties, but without a more complete treatment of the organic-lattice degrees of freedom, significant areas of the excited-state landscape remain challenging to explore. Examples include the dielectric screening of the cations,[18] as well as the thermal motion of cation molecules, which is known to affect excited-state properties[23, 24] such as photoluminescence lifetimes[25] and lead to significant distortions of the inorganic lattice.[26]

In *GW* and *GW*-BSE calculations, the main bottleneck is typically the calculation of the frequency-dependent and non-local inverse dielectric matrix, $\varepsilon^{-1}(q,\omega)$, within the random phase approximation (RPA),[27, 28] which scales as $O(N^4)$ or $O(N^3 \log N)$ with the number of electrons N in conventional plane-wave approaches and is essential for including non-local and dynamical screening effects beyond the standard capabilities of DFT or hybrid DFT.[15] The dielectric matrix is obtained from the non-interacting polarizability matrix, $\chi^0(q,\omega)$, by

$$\varepsilon_{GG'}(q,\omega) = \delta_{GG'} - v(q+G)\chi^0_{GG'}(q,\omega)$$
$$(1)$$

where $\chi^0_{GG'}(q,\omega)$ is calculated in the RPA from a sum over valence/conduction state pairs; $v(q+G)$ is the bare Coulomb potential in reciprocal space; q is a wavevector describing the momentum transfer; and G is a reciprocal lattice vector.[27, 28] As the noninteracting polarizability is linear for independent components of a chemical system, a variety of approaches have been developed to integrate screening from environmental subsystems by summing the polarizabilities.[10, 29-39] This technique is well-justified when wavefunction hybridization between the constituents is small, as is the case when the subsystems interact through weak van der Waals interactions. In layered perovskites, bandedge states come from the sublattice of inorganic octahedra, with molecular cations contributing to less dispersive bands about 1eV from the bandedge, suggesting that the main role of the organic cations in the electronic and optical response is through dielectric screening.[18] However, despite their energetic separation, the organic and inorganic subspaces, are connected with a strong ionic bond, involving significant charge transfer between the sublattices (see SI), precluding a straightforward application of established polarizability separation schemes.

Here, we develop a generalized scheme, which we refer to as the ionic polarizability separation approximation with charge compensation (IPSA-2C), that allows us to separate the polarizability of an ionically bonded system and apply it to understand the role of the cations in the screening of layered hybrid organic/inorganic perovskites. This is done by separately calculating the polarizability of the anion and cation, while compensating for the broken bond using a formal charge approach to divide electrons in the bond over constituent subsystems. In layered perovskites, a further simplification is possible since each unit cell consists of four ionically-bonded molecular cations with different spatial orientations. We show that the minimal

polarizability building block in calculations on perovskites can be reduced to a single organic cation, allowing us to calculate the QP bandstructure and optical absorption spectra at as low as one seventh the computational cost of the direct calculation, while introducing insignificant error in the band gap and exciton binding energy and reducing memory requirements by a factor of 1/2 in our implementation. We derive an effective 2D dielectric function and show that non-local screening from the molecular cations, which is included in our scheme but cannot be trivially captured by model dielectric functions, is essential for describing the screening environment. Moreover, our method scales to supercells composed of multiple perovskite unit cells at virtually no additional computational cost and allows for improved reusability of computed dielectric matrices across different perovskite systems.

We start by performing full one-shot *GW*-BSE calculations, as implemented in the BerkeleyGW software package,[15] on top of DFT calculations in the Perdew-Burke-Ernzerhof (PBE) parametrization of the generalized gradient approximation[40], as implemented in the Quantum Espresso software package.[41, 42] We use this framework to obtain QP bandstructures and absorption spectra of a series of n=1 RP perovskites, A_2PbBr_4 (A = ethylammonium (EA), butylammonium (BA), phenylmethylammonium (PMA), and naphthalenemethylammonium (NMA)). All computations are performed using optimized norm-conserving Vanderbilt pseudopotentials[43, 44] and a fully-relativistic spinor formalism due to the strong spin-orbit effects in lead halide perovskites.[45-47] Frequency-dependence of the screening is incorporated through the Godby-Needs plasmon pole model.[48] Calculation parameters may be found in the SI. Then, another set of calculations is performed using the IPSA-2C approach. In IPSA-2C, we perform separate mean field calculations on the system's organic and inorganic subsystems using

appropriate background charge compensation, significantly reducing the time to obtain ε^{-1} by dividing up the total number of bands summed over between the subsystems without sacrificing convergence (see SI). In the A_2PbBr_4 case, consideration of formal charges confirms that approximately one electron from each -NH_3-bearing molecule is transferred into the inorganic sublattice (see SI) so that the full non-interacting polarizability is approximated as $\chi_{full}^0 \approx \chi_{PbBr_4 + 2e^{-}} + \chi_{A_2 - 2e^{-}}$, where $PbBr_4 + 2e^{-}$ describes the inorganic sublattice with two added electrons per $PbBr_4$ formula unit and $A_2 - 2e^{-}$ describes the organic sublattice with two removed electrons per A_2 formula unit. The noninteracting polarizabilities of the two subsystems are summed to construct the noninteracting dielectric matrix, which is then inverted. The direct *GW*-BSE calculations and the IPSA-2C calculations are compared to calculations on model structures in which the A-site cations are replaced with Cs atoms, referred to as $Cs^A_2PbBr_4$. The Cs^A calculations provide a comparison to a fully inorganic system of quantum wells separated by vacuum, showing both the relative performance of the IPSA-2C method and giving insight into the importance of molecular screening and local-field effects.

Figs. 1a-b show the QP bandstructures of $(EA)_2PbBr_4$ and $(NMA)_2PbBr_4$ calculated using the three different approaches (see SI for $(BA)_2PbBr_4$ and $(PMA)_2PbBr_4$), and Fig. 1c presents a numerical comparison of the QP bandgaps of all species. The IPSA-2C approach replicates the QP bandstructure accurately for all structures, especially in the vicinity of the $PbBr_4$-centered valence and conduction band edges, validating the base assumption that screening effects can be partitioned between organic and inorganic constituents. In contrast to the Cs substitution scheme, the IPSA-2C method gives more accurate results in the large interlayer distance/aromatic cation cases, which are relevant to chromophores of interest in many experiments.[49-52]

The Cs substitution method is relatively accurate for structures with smaller interlayer distances, where screening from inorganic layers dominates and the energy levels of the small hydrocarbons lie far from the bandedge. However, for the larger molecules, $Cs^{PMA}_2PbBr_4$ and $Cs^{NMA}_2PbBr_4$, the Cs substitution method fails to predict accurate QP energies because the screening of the aromatic cations is neglected, as noted in our earlier work.[18] It is also noteworthy that bands associated with the highest occupied molecular orbitals (HOMOs) and lowest unoccupied molecular orbitals (LUMOs) of the aromatic molecules appear in both the full and IPSA-2C calculations as flat bands lying 1-2 eV away from the band edge, while the Cs substitution method only reproduces bands with the character of the inorganic lattice. These flat bands have the largest relative QP energy errors for the IPSA-2C method, suggesting that organic-inorganic hybridization shifts the molecular orbital energies up to ~100 meV.

Fig. 2 shows the *GW*-BSE optical absorption spectra for the perovskites with the smallest and largest interlayer distance, $(EA)_2PbBr_4$ and $(NMA)_2PbBr_4$. Again, we see that IPSA-2C reproduces the full calculation almost exactly, including the exciton binding energies, giving 242 meV compared to 251 meV in the direct calculation of $(EA)_2PbBr_4$ and 342 meV compared to 311 meV in the direct calculation of $(NMA)_2PbBr_4$. Cs substitution, on the other hand, deviates considerably from the full spectrum in oscillator strengths, exciton binding energies, and higher energy spectral features. In particular, the overestimation of the exciton binding energy (434 meV for Cs^{EA} and 741 meV for Cs^{NMA}) results in an unphysically enhanced oscillator strength. Even in the short interlayer distance limit, significant features in the absorption spectra are only captured when the organic molecules are considered explicitly. One unusual feature is the large peak in the out-of-plane absorption of $Cs^{EA}_2PbBr_4$ near 4.5 eV and $Cs^{NMA}_2PbBr_4$ near 5.5 eV, characteristic of plasmon-like features typically found in the optical response of low-dimensional

8

systems along a confined direction.[53] Thus, when the organic molecule is neglected, the perovskite behaves more like a purely 2D material, leading to the appearance of unphysical optoelectronic features.

To develop a picture of how the screening effects captured in the IPSA-2C method compare to full and $Cs^A PbBr_4$ calculations, we define an effective 2D dielectric function, $\varepsilon_{2D}(q)$, describing the screening seen by two point charges sitting in the center of the inorganic plane and separated by a distance q in reciprocal space, following Ref. [54]. Fig. 3 shows the effective 2D dielectric function for the small and large interlayer distance limits.

We note substantially different small-q behaviors for the $(EA)_2 PbBr_4$ 2D dielectric functions. At distances on the scale of the thickness of the $PbBr_4$ layer (gray dashed line in Fig. 3a), the Cs^{EA} calculation underestimates the screening due to the absence of molecular screening. Conversely, the IPSA-2C method tracks closely with the full calculation in the small q limit, but it is more similar to the Cs^{EA} case in the large-q (or small distance) limit, when nearly all screening is within a single inorganic layer and molecular screening is minimally important.

The differences become much more pronounced in the $(NMA)_2 PbBr_4$ case due to more significant screening by the large aromatic cations. In the small-q limit, ε_{2D} is enormously different for the Cs^{NMA} calculation vs. the IPSA-2C and full calculations because the molecular screening becomes significant. In fact, the Cs^{NMA} dielectric function almost resembles that of a 2D material,[54] in which $\varepsilon_{2D}(q)$ dips downwards for small q's corresponding to screening lengths larger than the thickness of the 2D material, and eventually drops to 1 in the long wavelength (or strictly 2D) limit where $q \to 0$. In the Cs^{NMA} case, as $q \to 0$, $\varepsilon_{2D}(q)$ has an oscillatory behavior— swinging back up after dipping down. This increase in screening occurs at a screening length

comparable to the interlayer distance when the charges become screened by the neighboring lead halide layers. On the other hand, the IPSA-2C $\varepsilon_{2D}(q)$ tracks qualitatively with the full calculation while slightly underestimating the total screening, suggesting that interfacial effects increase the total system's screening. The three methods again perform more similarly in the large-q limit, with the full calculation capturing a minor increase in screening due to the interfacial bonding compared to the more approximate treatments.

While the comparison between the Cs^A model and IPSA-2C reveals the important role of the molecular screening, this raises the question of whether the molecular screening can be captured by some simpler model, such as the introduction of an effective molecular dielectric constant or dielectric function. To explore this, we further compare $\varepsilon_{2D}(q)$ from the fully non-local and *ab initio* IPSA-2C calculation with one where local field effects are neglected and the molecular screening is assumed to be homogeneous (yellow line in Fig. 3). The resulting effective 2D screening is hugely overestimated in the NMA case because the true dielectric effects of the NMA molecules are localized between inorganic layers, resulting in a highly inhomogeneous screening environment that cannot be fully captured without local field effects.

We have shown that the IPSA-2C method successfully incorporates molecular contributions to system screening. Here, the reduction in computational cost comes from the reduced number of electrons in each calculation of the polarizability, circumventing the high power-law scaling of *GW*-BSE. We can reduce the computational cost even further by applying the polarizability separation approximation to the smallest possible subsystems—separately treating each molecule in a perovskite unit cell. This is justified because the overlap between molecular orbitals on separate molecules is very small (see Fig. S1 in the SI), and thus, cross terms in the sum-over-bands in χ^0 for bands centered on different molecules will be negligible.

In the discussion thus far, the organic sublattice consists of four identical molecular cations of different orientations, suggesting a further possible simplification. A series of real-space rotations and translations applied to χ^0 of one molecule is in principle sufficient to reproduce the total molecular screening by all molecules in the unit cell. Since χ^0 is stored in a plane-wave basis with elements labeled by pairs ($q+G,q+G$'), we can make use of Fourier transform properties for translations and rotations: a translation by r in real space corresponds to a phase shift $e^{i(G-G')\cdot r}$ in k-space, and a rotation in real space corresponds to an identical rotation in k-space. In practice, one property of the two-point function χ^0 requires special treatment; the domain of $\chi^0(k,k')$ is restricted due to the periodicity of the crystal from all of k/k'-space to only k/k' pairs where $k=q+G$ and $k'=q+G'$. Starting from a discrete uniform q-grid, rotations of k and k' by an arbitrary angle will not necessarily satisfy this condition. To avoid this, we rotate the vectors **G**/**G'** by the determined angle while leaving the q vectors fixed—this corresponds approximately to rotating the images of the molecule in all unit cells in the crystal while leaving unit cell boundaries fixed, a physically-motivated procedure.

We use this single-molecule IPSA-2C approach to obtain GW bandstructures for $(PMA)_2PbBr_4$ and $(NMA)_2PbBr_4$, the two most computationally demanding structures in the conventional approach, and absorption spectra and $\varepsilon_{2D}(q)$ calculations of $(NMA)_2PbBr_4$, as a proof of principle (Fig. 4). We find that the single molecular cation method closely captures the results of the IPSA-2C approach with all molecules together. As χ^0 scales as $N_v \times N_c$, where N_v is the number of occupied and N_c the number of unoccupied bands, our single cation calculation achieves equivalent convergence to a calculation on four cations with ¼ the number of valence states and ¼ the number of conduction states in the limit of zero molecular hybridization, leading to a theoretical maximum speedup of a factor of 16 in the sum over states. The actual computational

speedup for the calculation of the full dielectric matrix changes from a factor of roughly 2x for IPSA-2C with all cations to a factor of roughly 7x with a single cation (Fig. 4c). In the $(NMA)_2PbBr_4$ case, the single cation calculation introduces an erroneous molecular energy band at around -0.8 eV, but the band edge is very well-described, suggesting that while care must be exercised, this picture is sufficient to capture low energy behaviors near the electronic and optical bandedge. The absorption spectra of $(NMA)_2PbBr_4$ are qualitatively similar (Figs. 4d-e), with the single molecule calculation giving an exciton binding energy of 315 meV compared to 311 meV in the direct calculation.

Finally, we show how the single molecule polarizability approximation changes the effective 2D dielectric function in Fig. 4f. We note that the $\varepsilon_{2D}(q)$ determined by the single-molecule and four-molecule IPSA-2C approaches are nearly identical in the large-q limit, but deviate as $q \to 0$ for screening lengths larger than the octahedral layer thickness by 4.9%. In return for this slight increase in error, this technique opens a route for studying the impact of orientationally disordered cations in halide perovskite systems.

We have developed a generalized technique, IPSA-2C, for accelerating *ab initio* MBPT calculations on layered perovskites, which relies on separating the polarizability of the full system into smaller polarizability building blocks defined to include a redistributed charge. We show that IPSA-2C can reproduce both the QP bandstructures and absorption spectra of a number of RP perovskites to high fidelity and that the minimal polarizability building block is a single organic molecule, resulting in a seven-fold speed-up for calculations of a single unit cell of an RP perovskite. We anticipate this method will generalize well to the wider class of ionically-bonded hybrid systems and will generalize at negligible cost to large, low-symmetry supercells of perovskites that are of great interest to the materials community but are otherwise

intractable at the *GW* level. Furthermore, our calculations clearly reveal the importance of non-

local screening effects from the molecular cations, which cannot be trivially captured by a model
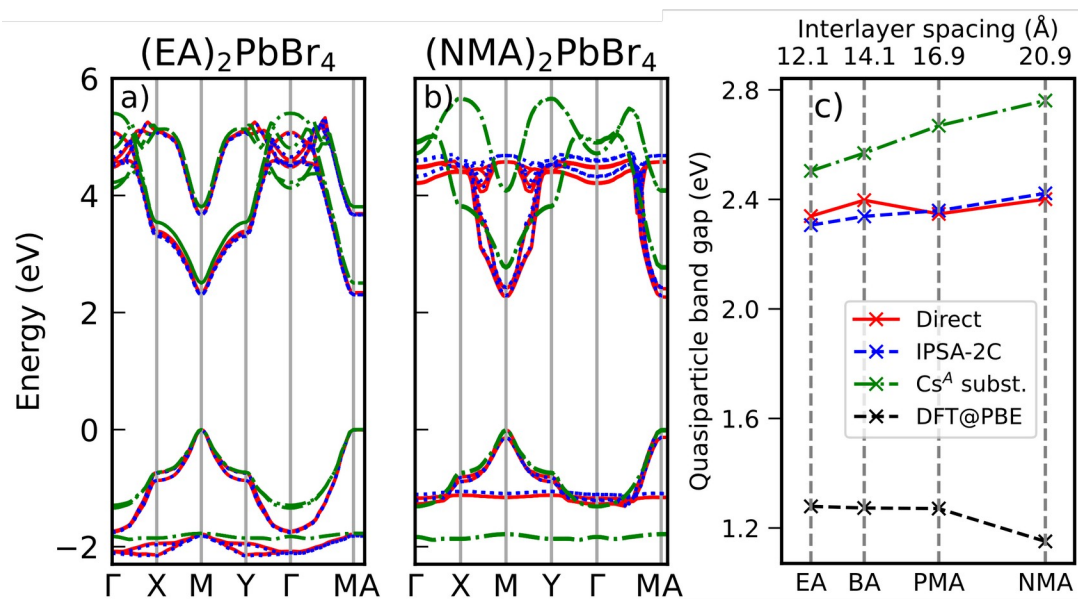
dielectric function.

FIGURES.

Figure 1. G_0W_0 QP bandstructures of $(EA)_2PbBr_4$ (a) and $(NMA)_2PbBr_4$ (b) in the direct calculation (red solid line), in the IPSA-2C method (blue dotted line), and with Cs^A cation substitution (green dashed line). G_0W_0 QP band gaps (c) for the four RP perovskite structures are labeled by their cation and the distance between stacked inorganic layers. Results shown as obtained from direct calculation (red), from the IPSA-2C approximation (blue), and with Cs^A cation substitution (green). Results from DFT@PBE shown in black.
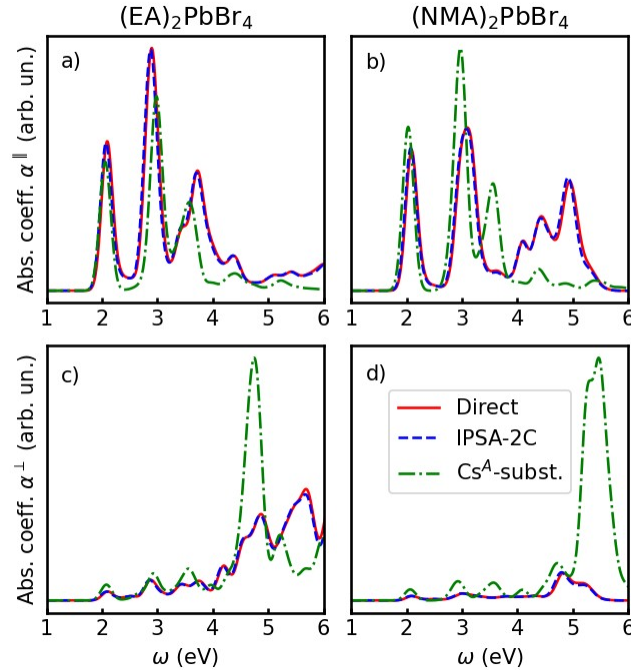
Figure 2. Comparison of G_0W_0-BSE optical absorption spectra of $(EA)_2PbBr_4$ and $(NMA)_2PbBr_4$ from direct calculation (solid red), with the IPSA-2C method (dashed blue), and with Cs^A cation substitution (dashed green). Plots are shown for light polarized along the in-plane (a, b) and out-of-plane (c, d) directions.
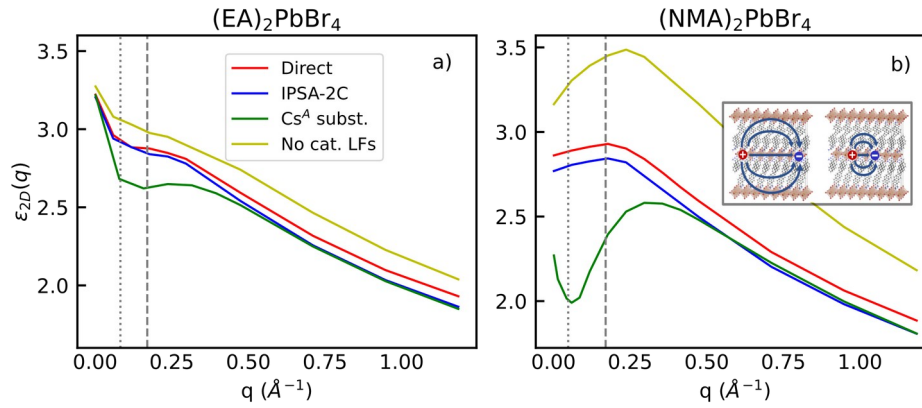
Figure 3. Effective 2D dielectric function $\varepsilon_{2D}(q)$ between two point charges within a single inorganic layer of $(EA)_2PbBr_4$ (a) and $(NMA)_2PbBr_4$ (b). Results shown for $\varepsilon_{2D}(q)$ as obtained by direct calculation (red), with the IPSA-2C method (blue), with Cs^A cation substitution (green), and within a partial IPSA-2C approach neglecting cation local fields, equivalent to treating the cations as a uniform dielectric medium (yellow). The dotted vertical line in each of (a) and (b) represents the inverse interlayer distance, and the dashed vertical line represents the inverse height of the $PbBr_4$ octahedra. In the inset in (b), a pictorial representation of the electric field lines screened by $\varepsilon_{2D}(q)$ is shown for large q (left) and small q (right).
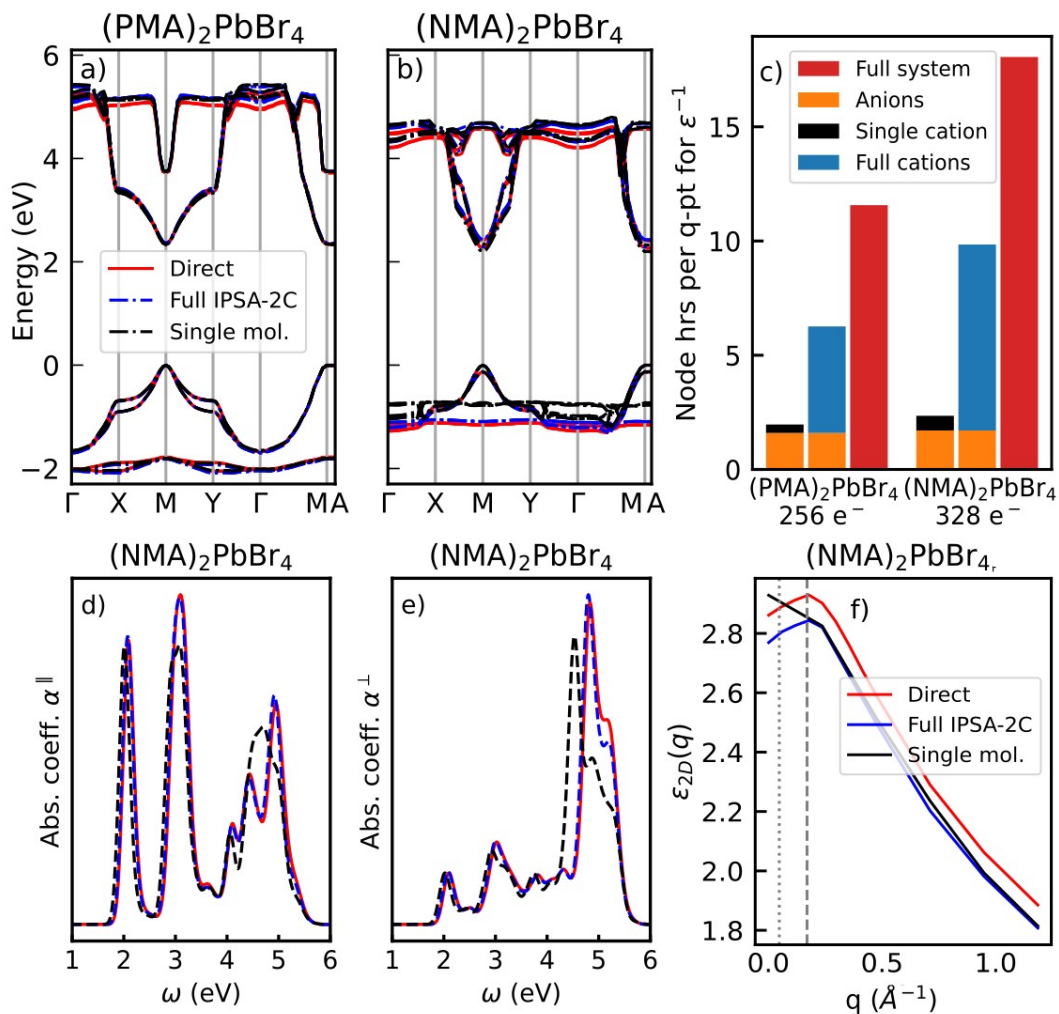
Figure 4. Comparison of results for the direct calculations (red), the IPSA-2C method with all four molecules per cell treated explicitly (blue), and the IPSA-2C single-molecule method (black), for *GW* quasiparticle bandstructures of $(PMA)_2PbBr_4$ (a) and $(NMA)_2PbBr_4$ (b), node hours to calculate ε^{-1} of $(PMA)_2PbBr_4$ and $(NMA)_2PbBr_4$ (see SI for benchmarking details) (c), in-plane (d) and out-of-plane (e) *GW*-BSE absorption spectra of $(NMA)_2PbBr_4$, and $\varepsilon_{2D}(q)$ of $(NMA)_2PbBr_4$ (f).

ASSOCIATED CONTENT

Supporting Information.

The following files are available free of charge.

Supporting Information: Images of unit cells for all model structures, Bader Charge Analysis of all model structures, direct/IPSA-2C/Cs^A bandstructures of all model structures, inorganic/organic lattice contributions to bandstructure of $(NMA)_2PbBr_4$, computational details. Refs. [14-16, 18, 40-44, 47, 48] are cited in the SI.

AUTHOR INFORMATION

Corresponding Author

*Dr. Diana Y. Qiu, diana.qiu@yale.edu

Present Addresses

-

Author Contributions

J.M. performed computations. J.M. and D.Y.Q. developed the methods described and wrote the manuscript. All authors had input and gave approval to the final version of the manuscript.

Notes

The authors declare no competing financial interest.

ACKNOWLEDGMENT

-

ABBREVIATIONS

EA, ethylammonium; BA, butylammonium; PMA, phenylmethylammonium; NMA, naphthylmethylammonium; QP, quasiparticle; RP, Ruddlesden-Popper; BSE, Bethe-Salpeter Equation

REFERENCES

[1]   Gharibzadeh S, Abdollahi Nejand B, Jakoby M, et al. Record open-circuit voltage wide-bandgap perovskite solar cells utilizing 2d/3d perovskite heterostructure. Advanced Energy Materials, 2019, 9: 1803699
[2]   Pedesseau L, Sapori D, Traore B, et al. Advances and promises of layered halide hybrid perovskite semiconductors. Acs Nano, 2016, 10: 9776-9786

[3]   Thomaz JE, Lindquist KP, Karunadasa HI, et al. Single ensemble non-exponential photoluminescent population decays from a broadband white-light-emitting perovskite. Journal of the American Chemical Society, 2020, 142: 16622-16631

[4]   Giorgi G, Yamashita K, Palummo M. Nature of the electronic and optical excitations of ruddlesden–popper hybrid organic–inorganic perovskites: The role of the many-body interactions. The Journal of Physical Chemistry Letters, 2018, 9: 5891-5896

[5]   Stoumpos CC, Cao DH, Clark DJ, et al. Ruddlesden–popper hybrid lead iodide perovskite 2d homologous semiconductors. Chemistry of Materials, 2016, 28: 2852-2867

[6]   Chen Y, Sun Y, Peng J, et al. 2d ruddlesden–popper perovskites for optoelectronics. Advanced Materials, 2018, 30: 1703487

[7]   Zheng Y, Niu T, Ran X, et al. Unique characteristics of 2d ruddlesden–popper (2drp) perovskite for future photovoltaic application. Journal of Materials Chemistry A, 2019, 7: 13860-13872

[8]   Blancon J-C, Tsai H, Nie W, et al. Extremely efficient internal exciton dissociation through edge states in layered 2d perovskites. Science, 2017, 355: 1288-1292

[9]   Katan C, Mercier N, Even J. Quantum and dielectric confinement effects in lower-dimensional hybrid perovskite semiconductors. Chemical Reviews, 2019, 119: 3140-3192

[10]   Latini S, Olsen T, Thygesen KS. Excitons in van der waals heterostructures: The important role of dielectric screening. Physical Review B, 2015, 92: 245123

[11]   Smith MD, Connor BA, Karunadasa HI. Tuning the luminescence of layered halide perovskites. Chemical Reviews, 2019, 119: 3104-3139

[12]   Li X, Hoffman JM, Kanatzidis MG. The 2d halide perovskite rulebook: How the spacer influences everything from the structure to optoelectronic device efficiency. Chemical Reviews, 2021, 121: 2230-2291

[13]   Braun M, Tuffentsammer W, Wachtel H, et al. Tailoring of energy levels in lead chloride based layered perovskites and energy transfer between the organic and inorganic planes. Chemical Physics Letters, 1999, 303: 157-164

[14]   Hybertsen MS, Louie SG. Electron correlation in semiconductors and insulators - band-gaps and quasi-particle energies. Physical Review B, 1986, 34: 5390-5413

[15]   Deslippe J, Samsonidze G, Strubbe DA, et al. Berkeleygw: A massively parallel computer package for the calculation of the quasiparticle and optical properties of materials and nanostructures. Computer Physics Communications, 2012, 183: 1269-1289

[16]   Rohlfing M, Louie SG. Electron-hole excitations and optical spectra from first principles. Physical Review B, 2000, 62: 4927-4944

[17]   Rohlfing M, Louie SG. Electron-hole excitations in semiconductors and insulators. Physical Review Letters, 1998, 81: 2312-2315

[18]   Filip MR, Qiu DY, Del Ben M, et al. Screening of excitons by organic cations in quasi-two-dimensional organic–inorganic lead-halide perovskites. Nano Letters, 2022, 22: 4870-4878

[19]   Molina-Sánchez A. Excitonic states in semiconducting two-dimensional perovskites. ACS Applied Energy Materials, 2018, 1: 6361-6367

[20]   Cho Y, Berkelbach TC. Optical properties of layered hybrid organic–inorganic halide perovskites: A tight-binding gw-bse study. The Journal of Physical Chemistry Letters, 2019, 10: 6189-6196

[21]   He Y, Galli G. Perovskites for solar thermoelectric applications: A first principle study of ch3nh3ai3 (a = pb and sn). Chemistry of Materials, 2014, 26: 5394-5400

[22]   Brivio F, Butler KT, Walsh A, et al. Relativistic quasiparticle self-consistent electronic structure of hybrid halide perovskite photovoltaic absorbers. Physical Review B, 2014, 89: 155204

[23]   Xu Q, Stroppa A, Lv J, et al. Impact of organic molecule rotation on the optoelectronic properties of hybrid halide perovskites. Physical Review Materials, 2019, 3: 125401

[24]   Liu S, Guo R, Xie F. The effects of organic cation rotation in hybrid organic-inorganic perovskites: A critical review. Materials & Design, 2022, 221: 110951

[25]   Lyu F, Zheng X, Li Z, et al. Spatiodynamics, photodynamics, and their correlation in hybrid perovskites. Chemistry of Materials, 2021, 33: 3524-3533

[26]   Egger DA, Rappe AM, Kronik L. Hybrid organic–inorganic perovskites on the move. Accounts of Chemical Research, 2016, 49: 573-581

[27]   Adler SL. Quantum theory of the dielectric constant in real solids. Physical Review, 1962, 126: 413-420

[28]   Wiser N. Dielectric constant with local field effects included. Physical Review, 1963, 129: 62-69

[29]   Ugeda MM, Bradley AJ, Shi S-F, et al. Giant bandgap renormalization and excitonic effects in a monolayer transition metal dichalcogenide semiconductor. Nature Materials, 2014, 13: 1091-1095

[30]   Lischner J, Vigil-Fowler D, Louie SG. Physical origin of satellites in photoemission of doped graphene: An ab initio gw plus cumulant study. Physical Review Letters, 2013, 110: 146801

[31]   Bradley AJ, M. Ugeda M, da Jornada FH, et al. Probing the role of interlayer coupling and coulomb interactions on electronic structure in few-layer mose2 nanostructures. Nano Letters, 2015, 15: 2594-2599

[32]   Qiu DY, da Jornada FH, Louie SG. Environmental screening effects in 2d materials: Renormalization of the bandgap, electronic structure, and optical spectra of few-layer black phosphorus. Nano Letters, 2017, 17: 4706-4712

[33]   Li L, Kim J, Jin C, et al. Direct observation of the layer-dependent electronic structure in phosphorene. Nature Nanotechnology, 2017, 12: 21-25

[34]   Naik MH, Jain M. Substrate screening effects on the quasiparticle band gap and defect charge transition levels in ${\mathrm{mos}}_{2}$. Physical Review Materials, 2018, 2: 084002

[35]   Andersen K, Latini S, Thygesen KS. Dielectric genome of van der waals heterostructures. Nano Letters, 2015, 15: 4616-4621

[36]   Xuan F, Chen Y, Quek SY. Quasiparticle levels at large interface systems from many-body perturbation theory: The xaf-gw method. Journal of Chemical Theory and Computation, 2019, 15: 3824-3835

[37]   Liu Z-F, da Jornada FH, Louie SG, et al. Accelerating gw-based energy level alignment calculations for molecule–metal interfaces using a substrate screening approach. Journal of Chemical Theory and Computation, 2019, 15: 4218-4227

[38]   Qiu DY, da Jornada FH, Louie SG. Solving the bethe-salpeter equation on a subspace: Approximations and consequences for low-dimensional materials. Physical Review B, 2021, 103: 045117

[39]   Cheng NLQ, Xuan F, Spataru CD, et al. Charge transfer screening and energy level alignment at complex organic–inorganic interfaces: A tractable ab initio gw approach. The Journal of Physical Chemistry Letters, 2021, 12: 8841-8846

[40]   Perdew JP, Burke K, Ernzerhof M. Generalized gradient approximation made simple. Physical Review Letters, 1996, 77: 3865-3868

[41]   Giannozzi P, Andreussi O, Brumme T, et al. Advanced capabilities for materials modelling with quantum espresso. Journal of physics: Condensed matter, 2017, 29: 465901

[42]   Giannozzi P, Baroni S, Bonini N, et al. Quantum espresso: A modular and open-source software project for quantum simulations of materials. Journal of physics: Condensed matter, 2009, 21: 395502

[43]   Hamann D. Optimized norm-conserving vanderbilt pseudopotentials. Physical Review B, 2013, 88: 085117

[44]   van Setten MJ, Giantomassi M, Bousquet E, et al. The pseudodojo: Training and grading a 85 element optimized norm-conserving pseudopotential table. Computer Physics Communications, 2018, 226: 39-54

[45]   Du M-H. Density functional calculations of native defects in ch3nh3pbi3: Effects of spin–orbit coupling and self-interaction error. The Journal of Physical Chemistry Letters, 2015, 6: 1461-1466

[46]   Barker BA. Electronic and optical properties of solids with strong spin-orbit coupling. 10822147 thesis. Ann Arbor: University of California, Berkeley, 2018

[47]   Barker BA, Deslippe J, Lischner J, et al. Spinor gw/bethe-salpeter calculations in berkeleygw: Implementation, symmetries, benchmarking, and performance. Physical Review B, 2022, 106: 115127

[48]   Godby RW, Needs RJ. Metal-insulator transition in kohn-sham theory and quasiparticle theory. Physical Review Letters, 1989, 62: 1169-1172

[49]   Xu Z, Lu D, Liu F, et al. Phase distribution and carrier dynamics in multiple-ring aromatic spacer-based two-dimensional ruddlesden–popper perovskite solar cells. ACS Nano, 2020, 14: 4871-4881

[50]   Zhou C, Chu Y, Ma L, et al. Photoluminescence spectral broadening, chirality transfer and amplification of chiral perovskite materials (rx-p-mbza) 2 pbbr 4 (x= h, f, cl, br) regulated by van der waals and halogen atoms interactions. Physical Chemistry Chemical Physics, 2020, 22: 17299-17305

[51]   Yang S, Niu W, Wang AL, et al. Ultrathin two-dimensional organic–inorganic hybrid perovskite nanosheets with bright, tunable photoluminescence and high stability. Angewandte Chemie International Edition, 2017, 56: 4252-4255

[52]   Dohner ER, Jaffe A, Bradshaw LR, et al. Intrinsic white-light emission from layered hybrid perovskites. Journal of the American Chemical Society, 2014, 136: 13154-13157

[53]   Grüning M, Marini A, Gonze X. Exciton-plasmon states in nanoscale materials: Breakdown of the tamm–dancoff approximation. Nano Letters, 2009, 9: 2820-2824

[54]   Qiu DY, da Jornada FH, Louie SG. Screening and many-body effects in two-dimensional crystals: Monolayer ${\mathrm{mos}}_{2}$. Physical Review B, 2016, 93: 235435